ADVANCED OPTICAL MATERIALS
www.advopticalmat.de

Self-Assembled Fluorophore-Based Probe for Efficient Detection of Endogenous Nitroreductase Activity in *Escherichia Coli*

Eiji Nakata, Yoshihiro Yukimachi, Hirokazu Kariyazono, Yoshijiro Nazumi, Futa Komatsubara, Mashal Asif, Yoshihiro Uto, and Hitoshi Hori*

Dedicated to the memory of the late professor Hitoshi Hori

Fluorescent probes are functional molecules whose fluorescent properties are transformed as a response to specific stimuli. Understanding the mechanisms of these transformations is essential for the design of these stimuli-responsive fluorescent probes. A rational design strategy has been developed to construct stimuli-responsive supramolecular cluster fluorescent probes. They operate by a new mechanism called self-assembly induced lactone formation (SAILac) to control the fluorescence properties of SNARF, an asymmetric xanthene fluorophore. Here, to expand SAILac applicability, the structure-activity relationship of the fluorophore scaffold is studied. SNARF-OBn(pNO$_2$), designed as nitroreductase-reactive fluorescent probe based on the SAILac mechanism, is selected as the initial structure. As the result of the structure-activity relationship studies, a new nitroreductase-reactive fluorescent probe, Rhodol-OBn(pNO$_2$), is created, having a superior signal-to-noise (S/N) ratio with higher reactivity toward nitroreductase than the original probe. By using Rhodol-OBn (pNO$_2$), the activity of endogenous nitroreductase in *Escherichia coli* is successfully detected.

1. Introduction

Fluorescent probes are essential tools in modern biological research, characterized by their ability to report the detection of specific stimuli that initiate alterations in their fluorescence.[1–6] These characteristics allow real-time monitoring of molecular dynamics in not only homogeneous test tube environments but also heterogeneous environments such as cells and individual organisms. Consequently, fluorescence detection using these probes plays a crucial role in advancing our understanding of biological systems.[2,7,8]

Fluorescent probes have been developed based on various mechanisms to detect a wide range of targets.[1,9] Among them, the turn-on type of fluorescent probes, which show strong fluorescence after the non-fluorescent form of the probe reacts with the target molecule, are useful because they are able to detect the target molecules with an unambiguous signal.[10,11] The fluorescence properties of stimuli-responsive probes not only change as a single molecule-based switch,[4,5,11,12] but can also be altered by the formation and deformation of supramolecular clusters created by the interactions between the probes or the fluorescent products themselves.[13] Several well-known supramolecular phenomena that influence the fluorescence properties of fluorophores include aggregation-caused quenching (ACQ)[8,14] and aggregation-induced emission (AIE).[15,16] Previously, we developed a rational design strategy to construct supramolecular cluster-based fluorescent probes which operate by a new mechanism called self-assembly induced lactone formation (SAILac) to control the fluorescence properties of seminapthorhodafluor (SNARF), which is classified as an asymmetric xanthene fluorophore with visible light excitation and fluorescence (**Figure 1a**).[6,17–19] It is known that xanthene fluorophores such as SNARF are in equilibrium between the fluorescent quinoid form and the non-fluorescent lactone form which has no absorption above 400 nm.[18,20–22] Although the non-fluorescent lactone form is generally not present in aqueous media, certain SNARF derivatives in which the phenolic substituent is protected by hydrophobic substituents such as the benzyl group were found to form self-assembled clusters of the non-fluorescent lactone (Figure 1b).[17,18] Furthermore, the self-assembled cluster can be equipped with different reactive properties according to the nature of the

E. Nakata, F. Komatsubara, M. Asif
Institute of Advanced Energy
Kyoto University
Gokasho, Uji, Kyoto 611-0011, Japan
E-mail: nakata@iae.kyoto-u.ac.jp
Y. Yukimachi, H. Kariyazono, Y. Nazumi, Y. Uto, H. Hori
Institute of Technology
Industrial and Social Sciences
Tokushima University Graduate School
Minamijosanjimacho 2, Tokushima 770–8506, Japan
The ORCID identification number(s) for the author(s) of this article can be found under https://doi.org/10.1002/adom.202402530

DOI: 10.1002/adom.202402530

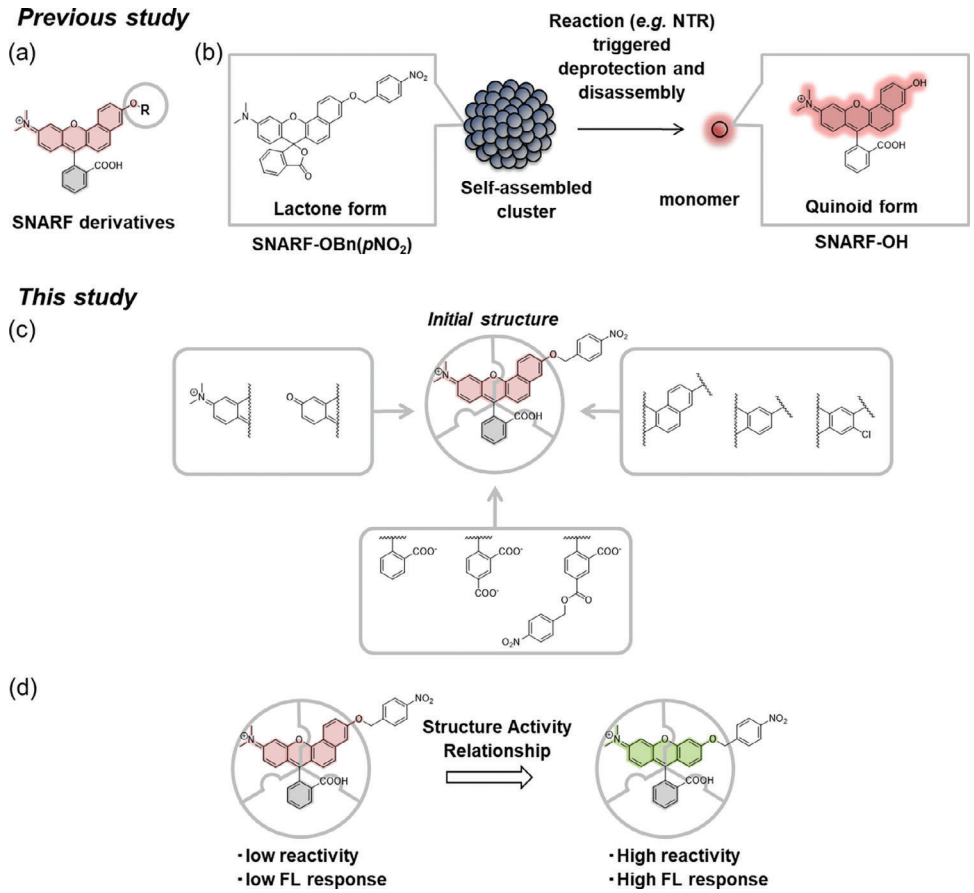

Figure 1. a,b) Previous studies based on the SAILac strategy with SNARF derivatives. (a) The structure-activity relationship study is based on the SNARF scaffold. SNARF derivatives, in which the phenolic group of SNARF was protected by various substituents, were studied. (b) Schematic illustration of the proposed mechanism of SAILac-based fluorescent probe (e.g., SNARF-OBn(pNO$_2$)). The entire scheme is shown in Figure S1a (Supporting Information). c,d) This study of the SAILac strategy uses different types of fluorophore scaffolds. (c) The strategy behind the structure-activity relationship study of xanthene-based fluorophores bearing the *p*-nitrobenzyl group. SNARF-OBn(pNO$_2$) was chosen as the initial structure. (d) The results of the structure-activity relationship study to obtain derivatives with high reactivity and a high fluorescence signal response.

substituents introduced.[18] We have demonstrated that the *p*-acetoxy-benzyl, *tert*-butyldiphenylsilyl, and *p*-nitrobenzyl groups impart esterase,[23] fluoride ion,[24] and nitroreductase reactivities (Figure 1a)[18,25] respectively. Thus, the design strategy of the fluorescent probe based on the SAILac mechanism was established as follows (Figure 1b): the self-assembled cluster of SNARF derivatives, existing as the non-fluorescent lactone protected by the reactive group of choice, was deprotected by reaction with the target molecules, dispersed, and fluoresced. Notably, compared to the well-known xanthene derivative aggregation state which simply induces spectral shifts in the absorption,[26] this system confers enhanced performance such as improved photostability and higher S/N ratios through the lack of SNARF absorption in the visible region combined with the deprotection-triggered disassembly and the resulting fluorescence.[5] However, the SAILac mechanism had only been applied to SNARF derivatives,[17,18] so relationship between the structure of the fluorophore and its ability to form the self-assembled cluster was not well-understood, making it unclear whether it could be applied to other fluorophore scaffolds. As the characteristics of the SAILac, it has been observed that there is a trade-off between reactivity and stability as the self-assembled SNARF derivative clusters showed lower reactivity than the monomeric forms of the probes while having higher stability toward undesired hydrolysis.[24] By better understanding how the structure of the fluorophore relates to self-assembly, one of our primary aims was to obtain a self-assembled cluster that has comparable reactivity to the dispersed fluorescent probe.

Here, we describe the development of the self-assembled fluorophore-based nitroreductase (NTR) probe as a representative example. The selective and efficient detection of NTR is of great importance,[16,27] since the activity of NTR has been known for decades and has been extensively studied in various systems such as bacteria, yeast, and hypoxic tumors.[28] As a result of the structure-activity relationship study (including SNARF derivatives and other xanthene derivatives) of the fluorophore scaffold (Figure 1c), we were able to better understand the self-assembled fluorescent probe cluster formation and the associated reactivities toward NTR to ultimately develop Rhodol-OBn(pNO$_2$) which maintains the reactivity toward NTR while having a superior S/N ratio compared to the monomeric counterpart (Figure 1d). By using Rhodol-OBn(pNO$_2$) as a NTR-selective fluorescent probe,

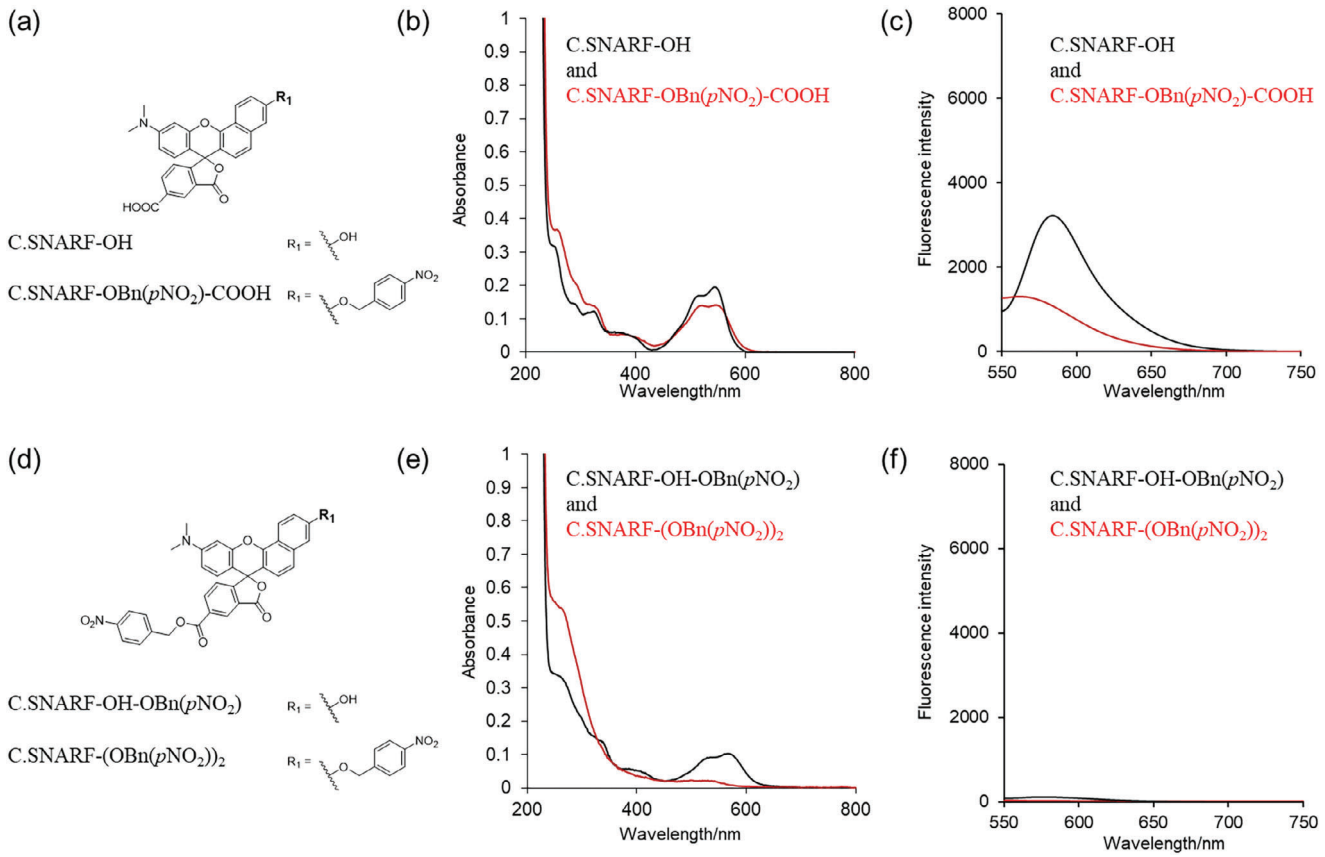

Figure 2. a,d) The molecular structures of C.SNARF derivatives. b,e) Absorption and c,f) fluorescence spectra (excited at 534 nm) of b,c) C.SNARF-OH (solid black line), and C.SNARF-OBn(pNO$_2$)-COOH (solid red line), e,f) C.SNARF-OH-OBn(pNO$_2$) (solid black line) and C.SNARF-(OBn(pNO$_2$))$_2$ (solid red line), respectively.[SNARF derivatives] = 10 μM in pH 5.0 10 mM Tris, HEPES, and acetate buffer.

endogenous NTR activity in *Escherichia coli* was successively detected.

2. Results

2.1. Comparison of the Structure and the Self-Assembled Cluster Formation Properties of *p*-Nitrobenzyl Group Modified C.SNARF-OH Derivatives

SNARF-OBn(pNO$_2$) (Figure S1b, Supporting Information), in which the phenolic group of SNARF-OH was protected by a p-nitrobenzyl group, exists as the self-assembled cluster under aqueous conditions (Figure S1c,d, Supporting Information) as reported previously.[17,18,25] Here, C.SNARF-OH derivatives (C.SNARF-COOH-OBn(pNO$_2$), C.SNARF-OH-OBn(pNO$_2$) and C.SNARF-(OBn(pNO$_2$)$_2$), in which the phenolic group and/or the carboxylic acid group of C.SNARF-OH were p-nitrobenzyl protected (**Figure** 2a,d), were designed and synthesized as shown in supporting information. The evaluation of the spectroscopic properties of C.SNARF-OH derivatives revealed that they produced absorption and fluorescence emission spectra distinct from those of C.SNARF-OH (Figure 2b–f). C.SNARF-OH showed maximum absorption and fluorescence emission around 548 and 585 nm at pH 5.0, respectively (Figure 2b,c; Table S1, Supporting Information).[18,21,22] C.SNARF-OBn(pNO$_2$)-COOH, of which the phenolic group was protected by a p-nitrobenzyl group while the carboxylic acid remains free, showed maximum absorption at 521 and 551 nm and fluorescence emission around 572 nm. Dynamic light scattering (DLS) measurements (Table S2, Supporting Information) and scanning electron microscopy (SEM) images (Figure S2b, Supporting Information) of C.SNARF-OBn(pNO$_2$)-COOH did not produce any peaks or any images of aggregation. The results indicate that C.SNARF-OBn(pNO$_2$)-COOH is present in its monomeric state in aqueous solution, though the reason for the blueshift in the absorption and fluorescence spectra is unclear. These results suggest that the presence of a hydrophilic substituent such as a carboxylic acid can prevent the formation of the self-assembled cluster. It should be noted the results are consistent with our previous study.[18,24] In the case of C.SNARF-OH-OBn(pNO$_2$), of which the carboxylic acid was protected by a p-nitrobenzyl group while having a free phenolic group, the absorption spectra showed maximum absorption around 571 nm but no fluorescence emission (Figure 2e,f). The maximum absorption of C.SNARF-OH-OBn(pNO$_2$) was significantly redshifted compared to that of C.SNARF-OH. The result suggests the formation of a head-to-tail type aggregate (J-type).[26] DLS measurements (Table S2, Supporting Information) and SEM images (Figure S2c, Supporting Information) of C.SNARF-OH-OBn(pNO$_2$) also support cluster formation. If C.SNARF-OH-OBn(pNO2) is

thought of as the scaffold of the fluorophore, the fluorophore modified with hydrophobic groups, such as *p*-nitrobenzyl, formed colored clusters that exhibit ACQ and may take on a different conformation than SAILac clusters.[8,14] C.SNARF-(OBn(pNO$_2$))$_2$, of which both the phenolic and the carboxylic acid groups were protected by a *p*-nitrobenzyl group, did not exhibit a significant absorption above 400 nm or any fluorescence emission (Figure 2e,f). These results were in good agreement with our previous studies where SNARF-OBn(pNO$_2$), the SNARF derivative that forms a self-assembled cluster, experiences the disappearance of absorption based on the SAILac mechanism.[17,18,23,24] DLS measurements of C.SNARF-(OBn(pNO$_2$))$_2$ showed particles with a mean diameter of 649.4 ± 149.9 nm as shown in Table S2 (Supporting Information). And SEM image of C.SNARF-(OBn(pNO$_2$))$_2$ showed the formation of clusters (Figure S2d, Supporting Information). These results give strong support for C.SNARF-(OBn(pNO$_2$))$_2$ self-assembled cluster formation. In total, these results suggest that the formation of the cluster can be controlled by modifying the fluorophore scaffold. C.SNARF-OBn(pNO$_2$)-COOH was present as the monomeric state in aqueous solution because of the hydrophilic carboxylic acid group in the fluorophore scaffold. On the other hand, C.SNARF-OH-OBn(pNO$_2$), of which the carboxylic acid group is protected by a hydrophobic *p*-nitrobenzyl group in the fluorophore scaffold, interestingly formed the colored cluster.[26] Finally, C.SNARF-(OBn(pNO$_2$))$_2$, of which the phenolic group was protected by *p*-nitrobenzyl group, unsurprisingly formed a cluster.

2.2. Comparison of the Nitroreductase Reactivity of *p*-nitroBenzyl Group-Modified C.SNARF-OH Derivatives

As we have reported previously,[17,18,25] SNARF-OBn(pNO$_2$) derived from SNARF-OH formed the self-assembled cluster having reactivity with nitroreductase (NTR) (**Figure 3a**; Figure S3a, Supporting Information). Here, the reactivities of NTR toward C.SNARF-OH derivatives having one or more *p*-nitrobenzyl groups (C.SNARF-OBn(pNO$_2$)-COOH, C.SNARF-OH-OBn(pNO$_2$) and C.SNARF-(OBn(pNO$_2$)$_2$) were compared to that of SNARF-OBn(pNO$_2$) (Figure 3; Table S3, Supporting Information). The absorption and fluorescence spectra of SNARF-OH and C.SNARF-OH derivatives were measured in the presence of NTR (Figure S3, Supporting Information) and the comparison of the time taken to reach half the maximum fluorescence intensity ($t_{1/2}$), and the maximum fluorescence change (I/I_0) are summarized in Table S3 (Supporting Information). In the case of SNARF-OBn(pNO$_2$), a time-dependent SNARF-OH derived absorption and fluorescence increase were observed (Figure S3b, Supporting Information). As shown in Figure 3b, the fluorescence increased gradually over 200 min with an I/I_0 of over 50, and $t_{1/2}$ was determined to be 60 min. In the case of C.SNARF-OH-OBn(pNO$_2$), the absorption spectra underwent a blueshift and the fluorescence spectra showed a significant increase (Figure S3d, Supporting Information) which plateaued within 100 min. I/I_0 and $t_{1/2}$ were determined to be 20 and 25 min, respectively. The results suggest that the J-type colored C.SNARF-OH-OBn(pNO$_2$) cluster[26] reacts with NTR, leading to the deprotected and disassembled cluster to produce the fluorescent C.SNARF-OH. On the other hand, the self-assembled cluster derived from C.SNARF-(OBn(pNO$_2$))$_2$ did not show any absorption or fluorescence change over a 200 min reaction (Figure S3e, Supporting Information). This indicates that the self-assembled cluster formed by C.SNARF-(OBn(pNO$_2$))$_2$ cannot react with NTR under these experimental conditions. It can be inferred from these results that C.SNARF-(OBn(pNO$_2$))$_2$ forms a sturdy and non-reactive cluster with strong hydrophobic interactions caused by introducing two *p*-nitrobenzyl groups. The absorption and fluorescence spectra of C.SNARF-OBn(pNO$_2$)-COOH treated with NTR showed a ratiometric absorption change and slight fluorescence enhancement (Figure S3c, Supporting Information). As confirmed in the previous section, C.SNARF-OBn(pNO$_2$)-COOH was present in the monomeric state in aqueous solution at pH 7.0. In addition, phenolic group-protected C.SNARF-OH derivatives such as C.SNARF-OBn(pNO$_2$)-COOH exhibit the fluorescence properties of the phenol by fixing the molecule in the phenol form. After the reaction with NTR, the released C.SNARF-OH recovers the equilibrium between phenol and phenolate. Thus, C.SNARF-OBn(pNO$_2$)-COOH would be expected to show a ratiometric spectral change. However, under the experimental conditions at pH 7.0, C.SNARF-OH mainly exists in the phenol form because the pKa of C.SNARF-OH is 7.6 (Table S1, Supporting Information).[21] Therefore, C.SNARF-OBn(pNO$_2$)-COOH did not show a significant ratiometric fluorescence change at pH 7.0 as shown in Figure S3c (Supporting Information). To confirm the result, the reaction of C.SNARF-OBn(pNO$_2$)-COOH with NTR was conducted at pH 8.0 in a separate experiment (Figure S4, Supporting Information). The time-dependent ratiometric absorption and fluorescence change were observed and the fluorescence-derived phenolate form of C.SNARF-OH (635 nm) reached a plateau within 20 min which is the same as C.SNARF-OBn(pNO$_2$)-COOH at pH 7.0 as shown in Figure S4c (Supporting Information). These results indicate that monomeric C.SNARF-OBn(pNO$_2$)-COOH can quickly reacts with NTR (($t_{1/2}$ < 5 min)), though with only a slight fluorescence spectral change at pH 7.0 ($I/I_0 = 1.5$). Among these SNARF derivatives, SNARF-OBn(pNO$_2$) showed the largest fluorescence enhancement (I/I_0 > 40 at 80 min), though with moderate reactivity with NTR ($t_{1/2}$ = 60 min) (Figure 3b,c; Table S3, Supporting Information).

2.3. Comparison of the Structure and the Self-Assembled Cluster Formation Properties of the *p*-Nitrobenzyl Group-Modified Xanthene Derivatives

To expand the self-assembled cluster formation strategy, different types of xanthene derivatives were designed and synthesized to be protected by a *p*-nitrobenzyl group on the phenolic moiety of the xanthene scaffold (e.g., Rhodol-OH, Rhodol-Cl-OH, Fluorescein-OH (Table S1, Supporting Information)) as shown in **Figure 4** and the supporting information. The evaluation of the spectroscopic properties of the xanthene derivatives (Rhodol-OBn(pNO$_2$), Rhodol-Cl-OBn(pNO$_2$), and Fluorescein-OBn(pNO$_2$)) revealed that they produced absorption and fluorescence emission spectra distinct from the original xanthene fluorophores (Rhodol-OH, Rhodol-Cl-OH, and Fluorescein-OH). Rhodol-OH, Rhodol-Cl-OH, and Fluorescein-OH showed

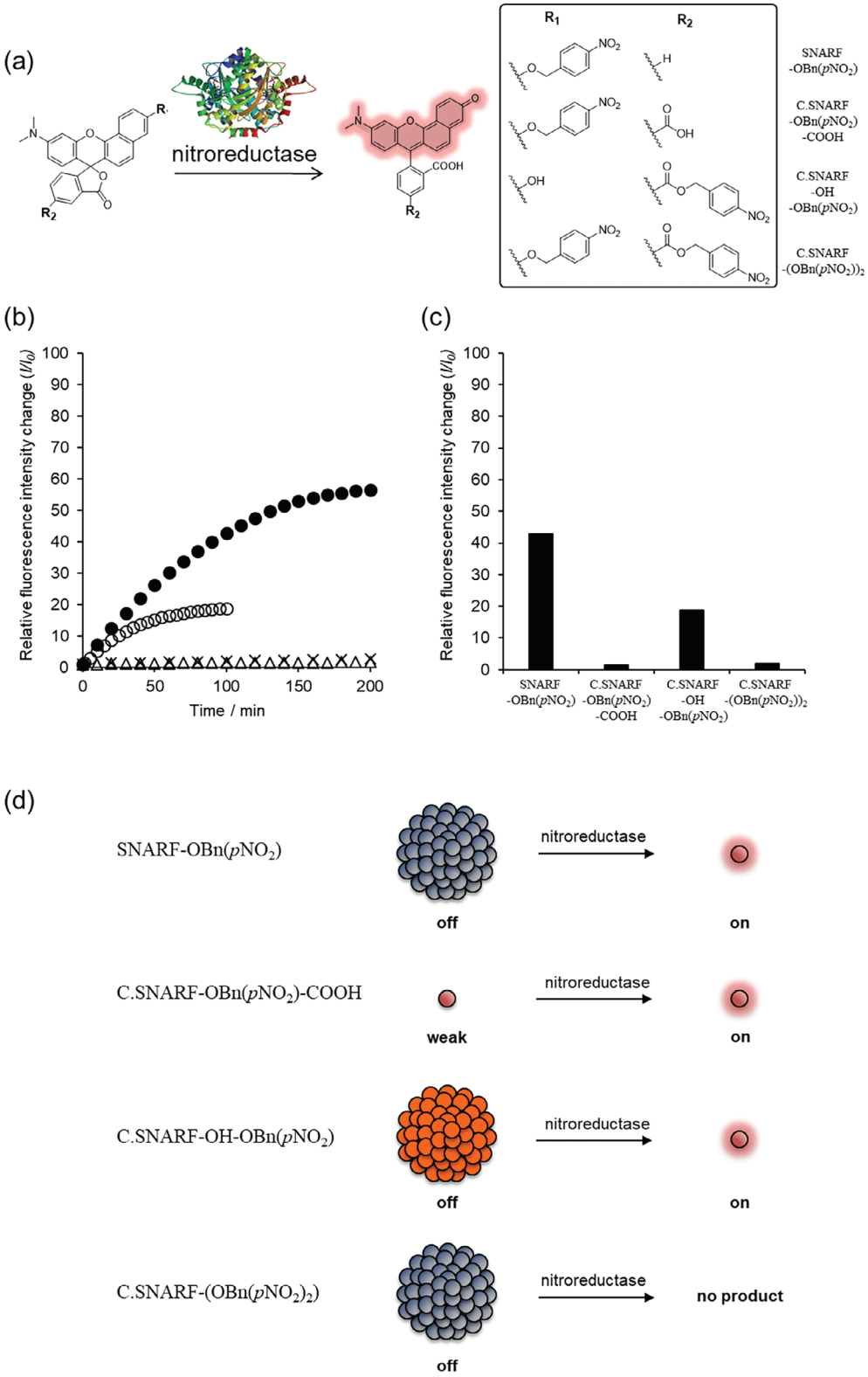

Figure 3. a) The reaction scheme of p-nitrobenzyl group-modified SNARF derivatives by NTR, b) The time plot of the relative fluorescence intensity changes (I/I_0) of SNARF-OBn(pNO_2) (black circle), C.SNARF-OBn(pNO_2)-COOH (white triangle), C.SNARF-OH-OBn(pNO_2) (white circle), and C.SNARF-$(OBn(pNO_2))_2$ (cross). c) Comparison of the relative fluorescence intensity changes of SNARF-OBn(pNO_2), C.SNARF-OBn(pNO_2)-COOH, C.SNARF-OH-OBn(pNO_2), and C.SNARF-$(OBn(pNO_2))_2$ after a 80 min reaction with NTR. d) An illustration of the reactions of SNARF derivatives with NTR and their outcomes.

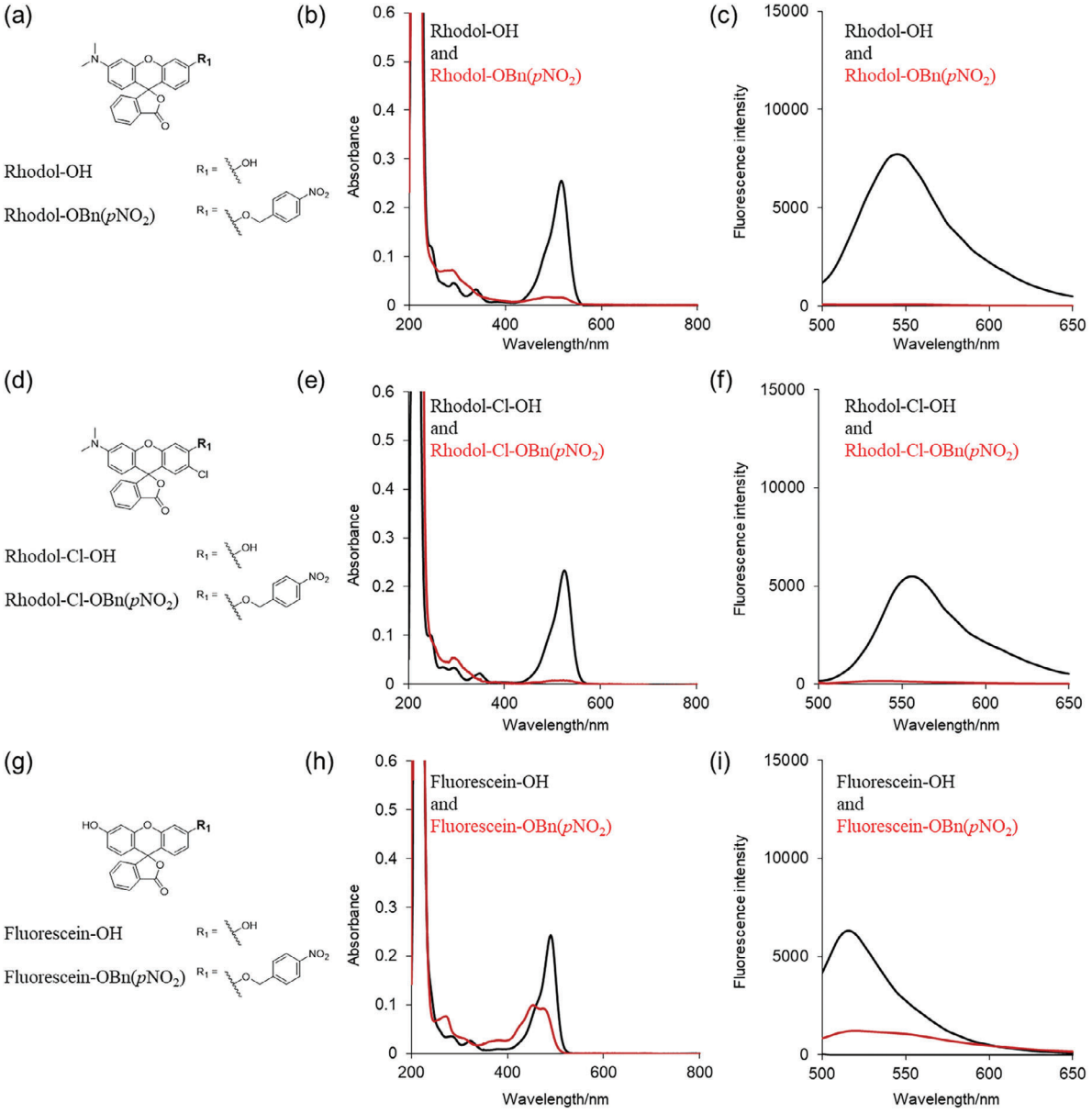

Figure 4. a,d,g) The molecular structure, b,e,h) the absorption spectra, and c,f,i) the fluorescence spectra (excited at 488 nm) of (a–c) Rhodol-OH (black line) and Rhodol-OBn(pNO$_2$) (red line), (d–f) Rhodol-Cl-OH (black line) and Rhodol-Cl-OBn(pNO$_2$) (red line), and (g–i) Fluorescein-OH (black line) and Fluorescein-OBn(pNO$_2$) (red line).[xanthene derivatives] = 10 μM in pH 7.0 10 mM Tris, HEPES, and acetate buffer.

maximum absorption around 517, 526, and 490 nm, respectively with fluorescence emissions around 548 559, and 514 nm at pH 7.0, respectively (Figure 4; Table S1, Supporting Information). However, Rhodol-OBn(pNO$_2$) and Rhodol-Cl-OBn(pNO$_2$) did not exhibit significant absorption above 400 nm or any fluorescence emission (Figure 4a–f). SEM images and DLS showed the formation of particles (Figure S5 and Table S4, Supporting Information). These results support the self-assembled cluster formation of Rhodol-OBn(pNO$_2$) and Rhodol-Cl-OBn(pNO$_2$) based on the SAILac mechanism[17,18] as they exhibited the lack of absorption. In the case of Fluorescein-OBn(pNO$_2$), maximum absorption was found at 454 and 472 nm and fluorescence emission around520 nm (Figure 4g–i). The values are consistent with the phenol form of Fluorescein-OH.[22] The results indicate that Fluorescein-OBn(pNO$_2$) is present in the monomeric state in aqueous solution.

2.4. Comparison of the Nitroreductase Reactivity of *p*-Nitrobenzyl Group Modified Xanthene Derivatives

The reactivity of xanthene derivatives (Rhodol-OBn(pNO$_2$), Rhodol-Cl-OBn(pNO$_2$), and Fluorescein-OBn(pNO$_2$)) with NTR (**Figure 5a**) were compared with that of SNARF-OBn(pNO$_2$). The absorption and fluorescence spectra of these derivatives were measured in the presence of NTR (Figure 5b,c; Figures S6–S8,

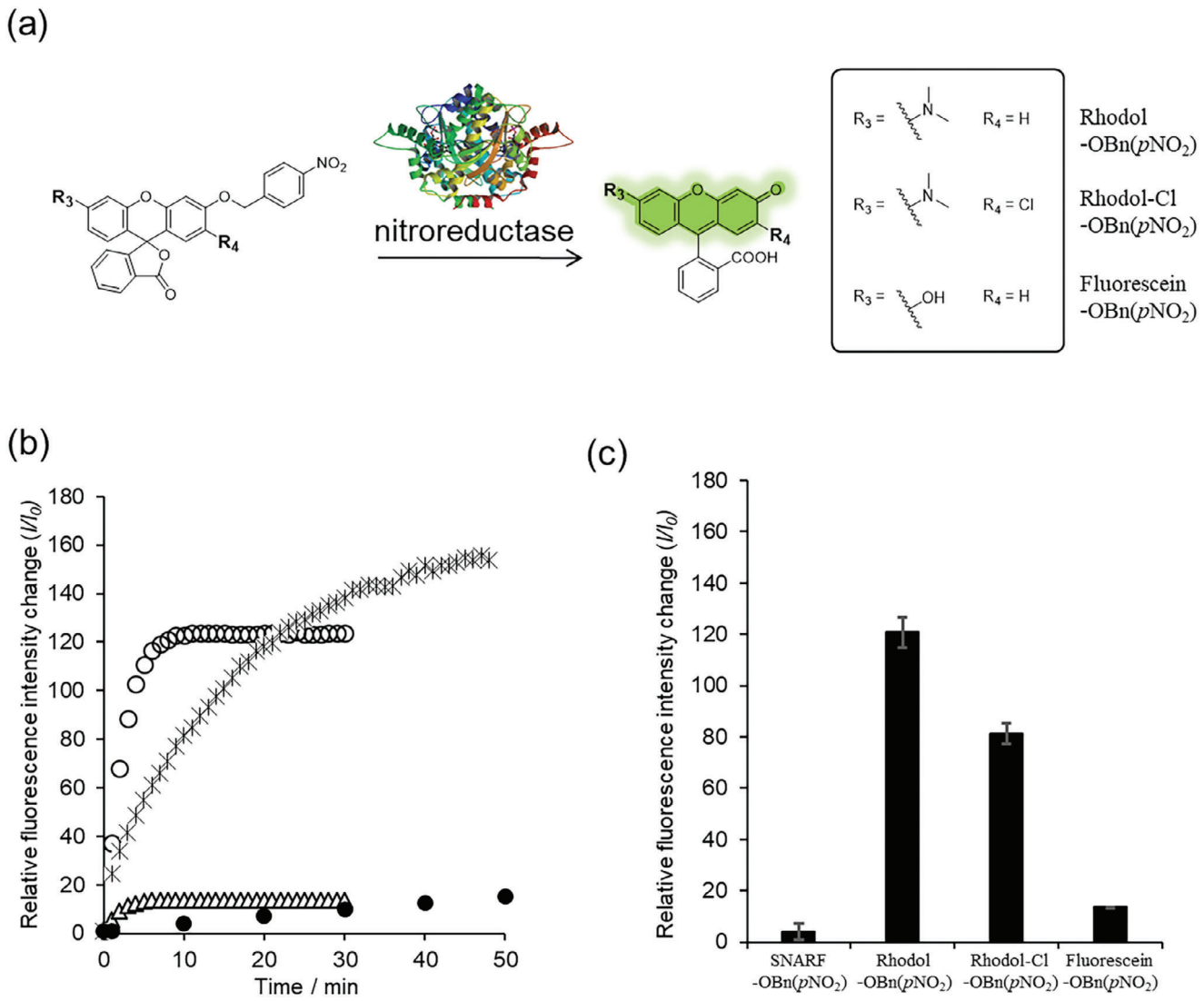

Figure 5. a) The reaction scheme of the p-nitrobenzyl group-modified xanthene derivatives deprotected by NTR. b) Time plot of the relative fluorescence intensity change (I/I_0) of SNARF-OBn(pNO$_2$) (black circle), Rhodol-OBn(pNO$_2$) (white circle), Rhodol-Cl-OBn(pNO$_2$) (asterisk), and Fluorescein-OBn(pNO$_2$) (white triangle). c) Comparison of the relative fluorescence intensity change of SNARF-OBn(pNO$_2$), Rhodol-OBn(pNO$_2$), Rhodol-Cl-OBn(pNO$_2$), and Fluorescein-OBn(pNO$_2$) after a 10 min reaction with NTR.

Supporting Information), and their $t_{1/2}$ and I/I_0 are summarized in Table S5 (Supporting Information). In the case of Rhodol-OBn(pNO$_2$) and Rhodol-Cl-OBn(pNO$_2$), a time-dependent absorption and fluorescence increase originating from Rhodol-OH (Figure S6, Supporting Information) and Rhodol-Cl-OH (Figure S7, Supporting Information) was observed. The fluorescence of Rhodol-OBn(pNO$_2$) quickly increased and reached a plateau within 10 min ($t_{1/2}$ < 2 min). The maximum fluorescence change reached more than 120 (I/I_0 = 124) (Figure 5b; Table S5, Supporting Information). Compared to SNARF-OBn(pNO$_2$) (plateau reached around 200 min ($t_{1/2}$ = 60 min) and I/I_0 = 56, Table S5, Supporting Information), Rhodol-OBn(pNO$_2$) showed rapid reactivity toward NTR and significant fluorescence enhancement. Rhodol-Cl-OBn(pNO$_2$) also showed faster reactivity (plateau reached around 50 min ($t_{1/2}$ = 10 min)) than SNARF-OBn(pNO$_2$) with a significant fluorescence increase (I/I_0 = 154), which was greater than that of Rhodol-OBn(pNO$_2$) as well. On the other hand, Fluorescein-OBn(pNO$_2$), which is present in the monomeric state in aqueous solution, showed rapid reactivity (plateau reached within 5 min ($t_{1/2}$ < 2 min)) and moderate fluorescence enhancement (I/I_0 = 14). Furthermore, the pH effect and the influence of various potentially biorelevant interferents on the detection of NTR activity are demonstrated in Figures S9 and S10 and Notes S1 and S2 (Supporting Information), respectively. Next, the kinetic parameters of the compounds (Rhodol-OBn(pNO$_2$), Rhodol-Cl-OBn(pNO$_2$), SNARF-OBn(pNO$_2$), and Fluorescein-OBn(pNO$_2$)) were determined, respectively (Figure S11, Table S6 and Note S3, Supporting Information). By comparing the apparent k_{cat}/K_m values, the self-assembled cluster derived from Rhodol-OBn(pNO$_2$) (k_{cat}/K_m = 3900 ± 300 $M^{-1}s^{-1}$) has a similar reactivity with the Fluorescein-OBn(pNO$_2$) (k_{cat}/K_m = 4000 ± 500 $M^{-1}s^{-1}$), which

exists in the monomeric state. On the other hand, Rhodol-Cl-OBn(pNO$_2$) (k_{cat}/K_m = 830 ± 200 M^{-1}s^{-1}) and SNARF-OBn(pNO$_2$) (k_{cat}/K_m = 25 ± 2.0 M^{-1}s^{-1}) have relatively slow reactivity. These results are consistent with the results based on the comparison of $t_{1/2}$ (Table S5, Supporting Information). Based on these results, self-assembled Rhodol-OBn(pNO$_2$) showed sufficient reactivity toward NTR which was comparable to that of monomeric Fluorescein-OBn(pNO$_2$) with superior fluorescence enhancement.

2.5. Endogenous Nitroreductase Activity in *E. coli* Monitored by Self-Assembled Rhodol-OBn(pNO$_2$) and SNARF-OBn(pNO$_2$)

The endogenous nitroreductase activity in *Escherichia coli* (*E. coli*) was directly monitored using Rhodol-OBn(pNO$_2$) or SNARF-OBn(pNO$_2$), both of which formed stable self-assembled clusters to react with NTR (**Figure 6**). First, DH5α, well-known as a *E. coli* K-12 derivative, was selected for use. A confluent *E. coli* cell culture and a five-fold concentrated culture were mixed with Rhodol-OBn(pNO$_2$) or SNARF-OBn(pNO$_2$) and their time-dependent fluorescence intensity change was monitored (Figure 6b,c). In the case of Rhodol-OBn(pNO$_2$), a significant *E. coli* concentration-dependent difference in the fluorescence increase was observed within the first 100 min and the fluorescence increased linearly over 500 min (Figure 6b). On the other hand, in the case of SNARF-OBn(pNO$_2$), little difference in the SNARF fluorescence was observed in the first 100 min and a slight difference from the control was observed only after a 500 min incubation (Figure 6c). The result was consistent with the previous finding that Rhodol-OBn(pNO$_2$) (I/I_0 = 124, $t_{1/2}$ < 2 min) has greater potential to monitor NTR reactivity in the test tube than SNARF-OBn(pNO$_2$) (I/I_0 = 56, $t_{1/2}$ = 60 min) (Table S5, Supporting Information). Next, the endogeneous nitroreductase activity of BL21(DE3) cells, which is known as a *E. coli* B strain derivative, and that of DH5α cells were compared by using Rhodol-OBn(pNO$_2$) and SNARF-OBn(pNO$_2$) (Figure 6d,e). A confluent *E. coli* culture of DH5α and BL21(DE3) cells were mixed with Rhodol-OBn(pNO$_2$) or SNARF-OBn(pNO$_2$) and their fluorescence intensities were quantified by gel imager as shown in Figure S12 (Supporting Information). The reaction yield of Rhodol-OBn(pNO$_2$) or SNARF-OBn(pNO$_2$) was determined from the calibration curve (Figure S12b, Supporting Information) obtained from different ratios of Rhodol-OBn(pNO$_2$) and Rhodol-OH or SNARF-OBn(pNO$_2$) and SNARF-OH, respectively. After a 3 h incubation with BL21(DE3) or DH5α cells, the reaction yield of Rhodol-OBn(pNO$_2$) or SNARF-OBn(pNO$_2$) with BL21(DE3) cells was shown to be significantly higher than that of DH5α cells (Figure 6d). In the case of both *E. coli* strains, Rhodol-OBn(pNO$_2$) showed a significantly higher reaction yield than that of SNARF-OBn(pNO$_2$) (Figure 6d) which is consistent with our previous findings (Figure 6b,c). Furthermore, Rhodol-OBn(pNO$_2$) with 1 mM NADPH showed a significantly higher reaction yield than in the absence of NADPH (Figure 6e), indicating that Rhodol-OBn(pNO$_2$) is a probe for the endogenous NADPH-dependent nitroreductases such as NfsA and/or NfsB. The same result was observed for SNARF-OBn(pNO$_2$) (Figure S12c, Supporting Information). Furthermore, the small numbers of *E. coli* detected by Rhodol-OBn(pNO$_2$) are shown in Figure S13 (Supporting Information). In the presence of 1 mM NADPH with 3 h incubation, Rhodol-OBn(pNO$_2$) significantly detected BL21(DE3) cells at an OD_{600} of 0.21, which is 1.7 × 10^8 cells mL^{-1}. Moreover, pretreatment of BL21(DE3) cells with the reductase inhibitor (Dicoumarol) showed an effect on Rhodol-OBn(pNO$_2$) reaction (Figure S14, Supporting Information), indicating the increment of fluorescence intensity was caused by the reaction of Rhodol-OBn(pNO$_2$) with endogenous reductase (Figure S15 and Note S4, Supporting Information). Moreover, pretreatment of BL21(DE3) cells with a reductase inhibitor (Dicoumarol) showed an effect on the Rhodol-OBn(pNO$_2$) reaction (Figure S14, Supporting Information), indicating the increase in fluorescence intensity was caused by the reaction of Rhodol-OBn(pNO$_2$) with endogenous reductase.

3. Discussion

Classification of the fluorophore scaffolds having a free phenol group (C.SNARF-OH, Fluorescein-OH, Rhodol-OH, Rhodol-Cl-OH, SNARF-OH, C.SNARF-OH-OBn(pNO$_2$)) based on the $LogD_{pH7.0}$(lactone) as a predictor of hydrophobicity ($LogD_{pH7.0}$(lactone) was defined as the LogD of the molecules in the lactone form at pH 7.0. See details in Figures S16 and S17 and Tables S7 and S8, Supporting Information) was carried out using the Pallas software. It was found that the hydrophobicity increased in the order C.SNARF-OH, Fluorescein-OH, Rhodol-OH, Rhodol-Cl-OH, SNARF-OH, C.SNARF-OH-OBn(pNO$_2$) (Figure S15, Supporting Information). Based on the absorption spectra shown in Figures 2, 4, and S1c (Supporting Information), all of the fluorophore scaffolds were present in the dispersed state in the buffer conditions (pH 7.0 10 mM Tris-Cl buffer) except for C.SNARF-OH-OBn(pNO$_2$). Though C.SNARF-OH-OBn(pNO$_2$) existed as the colored cluster, the cluster was dispersed in the presence of FBS-containing buffer (Figure S18 and Note S5, Supporting Information), indicating that C.SNARF-OH-OBn(pNO$_2$) formed the colored cluster, that is, the quinoid state cluster, through weak hydrophobic interactions. These results indicated the order of the hydrophobicity can be predicted based on the $LogD_{pH7.0}$(lactone). Next, the classification of these fluorophores, of which the phenol group was modified by Bn(pNO$_2$), was also carried out based on the $LogD_{pH7.0}$(lactone). It was found that the hydrophobicity increased in the order C.SNARF-OBn(pNO$_2$)-COOH, Fluorescein-OBn(pNO$_2$), Rhodol-OBn(pNO$_2$), Rhodol-Cl-OBn(pNO$_2$), SNARF-OBn(pNO$_2$), and C.SNARF-(OBn(pNO$_2$))$_2$ (Figure S17, Supporting Information), which is the same order as the fluorophore scaffold alone (Figure S16, Supporting Information). Based on the absorption spectra (Figures 2, 4, and S1c, Supporting Information) and DLS measurements (Tables S2 and S4, Supporting Information), the hydrophobic derivatives such as Rhodol-OBn(pNO$_2$), Rhodol-Cl-OBn(pNO$_2$), SNARF-OBn(pNO$_2$), and C.SNARF-(OBn(pNO$_2$))$_2$ formed the cluster as the colorless lactone form and the threshold between the dispersed and cluster states in the measurement buffer was present between Fluorescein-OBn(pNO$_2$) and Rhodol-OBn(pNO$_2$) (Table S8, Supporting Information). It should be noted that the order of the hydrophobicity of Bn(pNO$_2$)-modified xanthene fluorophores showed good correlation with the reactivity toward NTR. As an indicator of the reactivity toward NTR, the $t_{1/2}$ value was compared to the hydrophobicity

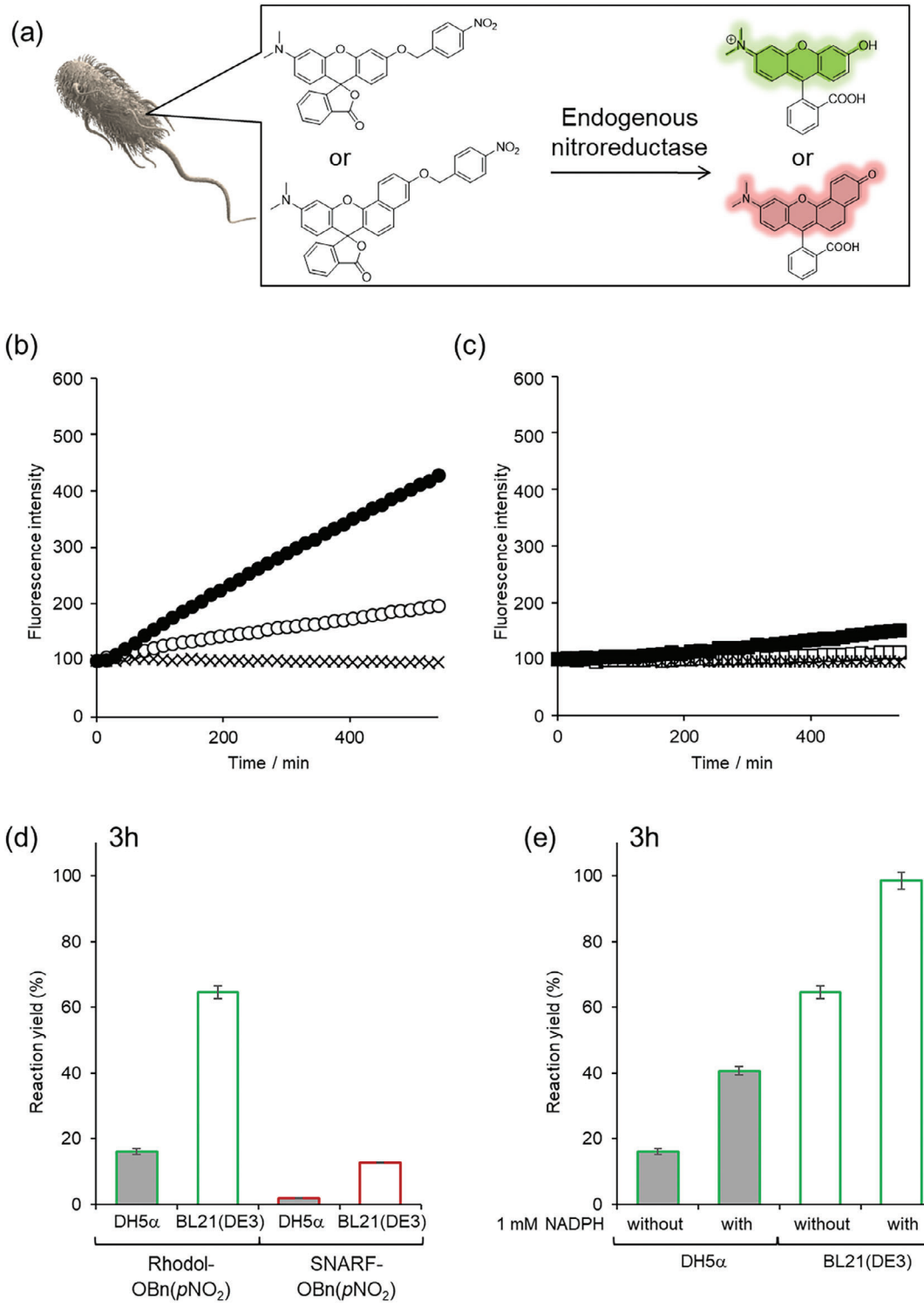

Figure 6. a) The reaction scheme of Rhodol-OBn(pNO$_2$) or SNARF-OBn(pNO$_2$) with endogenous nitroreductase in *E. coli*. b) Time plot of the relative fluorescence intensity change of Rhodol-OBn(pNO$_2$) incubated in a confluent (white circle) or five-fold concentrated (black circle) *E. coli* (DH5α) cell culture. The control (cross) was a solution of Rhodol-OBn(pNO$_2$) without bacteria. c) Time plot of the relative fluorescence intensity change of SNARF-OBn(pNO$_2$) incubated in a confluent (white square) or five-fold concentrated (black square) *E. coli* (DH5α) cell culture. The control (asterisk) was a solution of SNARF-OBn(pNO$_2$) without bacteria. d,e) Reaction yields of Rhodol-OBn(pNO$_2$) or SNARF-OBn(pNO$_2$) with endogenous nitroreductase in *E. coli* (DH5α or BL21(DE3)) after a 3 h incubation. (d) Comparison of the reaction yields of Rhodol-OBn(pNO$_2$) or SNARF-OBn(pNO$_2$) with different types of *E. coli* (DH5α or BL21(DE3)). (e) Comparison of the reaction yields of Rhodol-OBn(pNO$_2$) with different types of *E. coli* (DH5α or BL21(DE3)) with or without 1 mM NADPH.

defined by the $LogD_{pH7.0}$(lactone) (Tables S3, S5, and S8, Supporting Information). The $t_{1/2}$ value increased in the order Rhodol-OBn(pNO_2) (<2 min), Rhodol-Cl-OBn(pNO_2) (10 min), SNARF-OBn(pNO_2) (60 min), and C.SNARF-(OBn(pNO_2))$_2$ (no reactivity), the order of which showed good agreement with the order of hydrophobicity. These results indicate that the self-assembled fluorescent NTR probes with a reactive OBn(pNO_2)-containing xanthene fluorophore can be designed based on their hydrophobicities.

Among the self-assembled colourless cluster-based fluorescent NTR probes, Rhodol-OBn(pNO_2) has the highest reactivity toward NTR ($t_{1/2}$ < 2 min, k_{cat}/K_m = 3900 ± 300 $M^{-1}s^{-1}$) with good fluorescence change (I/I_0 = 124) and was used to detect the endogenous nitroreductase activity in *E. coli*. It is known that *E. coli* have numerous candidate nitroreductase genes (nfsA, nfsB, azoR, nemA, yieF, ycaK and mdaB).[29–31] Among them, NfsA and NfsB are the founding members of two families of NTRs that occur in a large number of bacteria.[32] SNARF-OBn(pNO_2), which has less reactivity and smaller fluorescence change than Rhodol-OBn(pNO_2), was used as the control of the self-assembled cluster type fluorescent probe. As shown in Figure 6b,c, Rhodol-OBn(pNO_2) showed higher reactivity and larger fluorescence increase than SNARF-OBn(pNO_2), which was consistent with the test tube experiment (Table S5, Supporting Information). The results indicate that Rhodol-OBn(pNO_2) performed better than SNARF-OBn(pNO_2) as a self-assembled fluorescent probe for monitoring endogenous nitroreductase activity in *E. coli*. Interestingly, there was a significant difference in the reaction yield of Rhodol-OBn(pNO_2) between the types of *E. coli*, that is, BL21(DE3) (*E. coli* B strain) had higher endogenous nitroreductase activity than DH5α (*E. coli* K strain). Furthermore, in the presence of high concentrations of NADPH (1 mM), a significantly higher reaction yield was observed than in the absence of NADPH supplementation. As was studied in-depth previously, both NfsA and NfsB showed NADPH dependent reactivity.[33] Therefore, it is possible that endogenous NfsA and/or NfsB were the main nitroreductase(s) to react with Rhodol-OBn(pNO_2) in *E. coli*.[31,34] However, based on the study of NTR-responsive prodrugs, there are still several other candidates such as NemA that may react with Bn(pNO_2).[29,35] Further experiments will be required to identify the specific enzymes that respond to these probes. Moreover, a wide range of nitroreductases are known to be present in various bacterial genomes including the ESKAPE pathogens (*Enterococcus faecium, Staphylococcus aureus, Klebsiella pneumoniae, Acinetobacter baumannii, Pseudomonas aeruginosa*, and *Enterobacter species*) which are pathogenic and harmful to human beings.[36] They are also present in some eukaryotes, especially those existing in hypoxic conditions.[37] Thus, nitroreductases have drawn great attention in recent years owing to their biotechnological, biomedical, environmental, and human impact.[38] Therefore, it becomes important to detect their activity within the cell.[39] Rhodol-OBn(pNO_2) has the potential to be applied to a wider range of bacterial nitroreductase detection. We expect Rhodol-OBn(pNO_2) to facilitate more detailed studies on the detection of bacterial nitroreductases in the future using differen cell types, which should help to classify and distinguish the differences in the series of bacteria.

4. Conclusion

Based on the structure-activity relationship study of xanthene fluorophores as nitroreductase probes bearing a p-nitrobenzyl group, we demonstrated that the SAILac mechanism could be applied not only to compounds with SNARF-OH as the scaffold but also to other xanthene fluorophores such as Rhodol-OH, Rhodol-Cl-OH, and C.SNARF-OH. By considering the hydrophobicity of the fluorophore scaffold, we could make accurate predictions and thereby design sophisticated derivatives having high reactivity toward the target. In particular, Rhodol-OBn(pNO_2), which has lower hydrophobicity than SNARF-OBn(pNO_2) but forms a self-assembled cluster based on the SAILac mechanism, showed higher reactivity toward NTR than SNARF-OBn(pNO_2). Additionally, Rhodol-OBn(pNO_2) showed a higher fluorescence increase and was able to more sensitively detect endogenous nitroreductase activity in *E. coli* than SNARF-OBn(pNO_2), which could just barely detect the endogeneous nitroreductase. With the expansion of this knowledge, we will rationally design SAILac mechanism-based fluorescent probes, which have the appropriate wavelengths, different fluorescence properties, and optimal reactivity toward various targets. Work in this direction is ongoing in our laboratory.

5. Experimental Section

Materials and Methods—General: ^{1}H-NMR spectra were recorded on a JEOL JNM-EX400 spectrometer (400 MHz) using tetramethylsilane as the internal standard. Chemical shifts were reported in ppm. Coupling constants were reported in Hz. HRMS was measured on a JOEL JMS-700 mass spectrometer using the FAB method. Reactions were monitored by analytical TLC using Merck Silica Gel 60 F254 aluminum plates. Column chromatography was performed on Kanto Chemical Silica Gel 60 N (230–400 mesh). All chemicals were purchased from Wako Pure Chemical Industries, Ltd (Osaka, Japan), Kanto Chemical Co., Inc. (Tokyo, Japan), Tokyo Chemical Industry Co., Ltd (Tokyo, Japan), Sigma-Aldrich Japan (Tokyo, Japan), or Invitrogen (Tokyo, Japan).

Materials and Methods—Synthesis of Xanthene Derivatives and Preparation of Stock Solution: The synthetic methods and characterization data were previously described for SNARF-OH, C.SNARF-OH, and SNARF-OBn(pNO_2).[18,23–25] The details of the synthetic methods and characterization data for C.SNARF-(OBn(pNO_2)$_2$, C.SNARF-(OBn(pNO_2)-OH, C.SNARF-OH-(OBn(pNO_2), Rhodol-OBn(pNO_2), Rhodol-Cl-OBn(pNO_2) and Fluorescein-OBn(pNO_2) were described here in the Supporting information. Their stock solutions (2 mM DMSO) were prepared and used in subsequent experiments by diluting with the assay buffer.

Materials and Methods—Calculation of the logD_{pH}: The $logD_{pH}$ values were determined using Pallas software. $LogD_{pH7.0}$(lactone) and Log $D_{pH7.0}$(quinoid) indicate the $logD_{pH}$ of the lactone and the quinoid forms, respectively, of xanthene fluorophores at pH 7.0.

Materials and Methods—Absorption Spectrophotometry: Absorption spectra of xanthene derivatives were measured in 10 mM Tris-HCl at pH 7.0 or pH 5.0 at room temperature. Absorption spectra were recorded on a U-3300 spectrometer (Hitachi), UV-2550 spectrometer (Shimadzu), or Infinit M200 (Tecan).

Materials and Methods—Fluorescence Spectrophotometry: Fluorescence spectra of SNARF derivatives were measured with excitation at 534 nm in 10 mM Tris-HCl buffer at pH 7.0 or pH 5.0 at room temperature. Fluorescence spectra were recorded on a F-4500 spectrometer (Hitachi), F-7000 spectrometer (Hitachi) or Infinit M200 (Tecan).

Materials and Methods—Absolute Fluorescence Quantum Yield Measurement: The absolute fluorescence quantum yields were determined at room temperature on a Quantaurus QY (C11347-11, Hamamatsu) equipped with an integrating sphere.

Materials and Methods—DLS Analysis: Dynamic light scattering (DLS) measurements were taken by placing xanthene derivatives in 10 mM Tris-HCl buffer at pH 7.0. The DLS was measured with a DLS-7000DL (Otsuka Electronics).

Materials and Methods—SEM Imaging: The xanthene derivatives (10 μM) in distilled water were dropped on a glass plate (9 mm x 9 mm) and dried at room temperature for 24 h. Pt–Pd coating was applied for 30 s. SEM images were recorded on a S-4700 Field-Emission Scanning Electron Microscope (Hitachi). Ion beam spattering was performed on an E-1020 ion sputterer (Hitachi).

Materials and Methods—Bioreductive Activation of Nitroaromatic Residue by Nitroreductase: Nitroreductase from *E. coli* (NTR, NfsB) was purchased from SIGMA Co. ltd. The preincubated solution of xanthene derivatives (5 μM) and NADPH (500 μM) in the assay buffer (50 mM Tris–HCl buffer (pH 7.0 or pH 8.0)) at 20 ± 1 °C was mixed with NTR (final concentration: 0 or 2.0 U mL^{-1}). The fluorescence spectra and UV–vis spectra were monitored during the appropriate reaction time.

Materials and Methods—Kinetic Assay: A calibration curve of fluorescence intensity versus concentration of Rhodol-OH (the enzymatic reaction product of Rhodol-OBn(*p*NO_2)) was created by measuring the fluorescence intensity of 0.78, 1.6, 3.1, 6.3, 13, 25, and 50 μM of in 50 mM Tris–HCl buffer (pH 7.0) at 20 ± 1 °C. The enzyme reaction for the kinetic study was performed in 50 mM Tris–HCl buffer (pH 7.0) containing NADPH (500 μM), NTR (20 μg mL^{-1}) and Rhodol-OBn(*p*NO_2) (0.78–50 μM) at 20 ± 1 °C. The reaction was initiated upon the addition of NADPH, and the change in fluorescence intensity was monitored (excitation wavelength: 480 nm, emission wavelength: 550 nm). The initial velocity was calculated from the change in fluorescence intensity with the calibration curve, and plotted against substrate concentration. The results were fitted to the Michaelis–Menten Equation (1) using GraphPad Prism software to calculate the apparent kinetic parameters.

$$V_{ini} = V_{max}[S]/(K_m + [S]) \quad (1)$$

where V_{ini} = initial velocity and[S] = substrate concentration. k_{cat} was derived from the following Equation (2).

$$k_{cat} = V_{max}/[E]_0 \quad (2)$$

where$[E]_0$ = molar enzyme concentration (0.83 μM). k_{cat} was calculated using the molecular weight of NTR (24000).

The kinetic parameters of Rhodol-Cl–OBn(*p*NO_2), SNARF-OBn(*p*NO_2), and Fluorescein-OBn(*p*NO_2) were determined the same manner.

Materials and Methods—Bioreductive Activation of Nitroaromatic Residue by Endogenous Nitroreductase in E. coli: The initial stock culture of *Esterichia coli* (DH5α or BL21(DE3) transformed with the pET30a plasmid) was made by reconstituting lyophilized bacteria in warm LB medium (Tryptone 10 g L^{-1}, Yeast Extract 5g L^{-1}, Sodium Chloride 10 g L^{-1}) with 30 μg mL^{-1} Kanamycin sulfate and grown overnight at 37 °C and 200 rpm to an optical density at 600 nm (OD_{600}) of ≈2.0. The concentration of *E. coli* cell cultures was calculated by OD_{600} (1.0 of OD_{600} = 8 × 10^8 cells mL^{-1})[40] For preparation of the five-fold concentrated *E. coli* solution, the bacteria solution (1 mL) was centrifuged at 3000 rpm for 10 min and 800 μl of the supernatant was removed. For the preparation of different OD_{600} of *E. coli*, the bacteria solution (1 mL) was diluted by LB medium and measured OD_{600}. For preparation of *E. coli* in PBS buffer, the bacteria solution (1 mL) was centrifuged at 300 rpm for 10 min and the supernatant was exchanged to PBS buffer and measured OD_{600} (2.1 of OD_{600} samples were used). For preparation of a reductase inhibitor (dicoumarol) treated *E. coli*, the bacteria solution (1 mL) was mixed with dicoumarol (final concentration 100 μM). 5 μl of a 2 mM DMSO stock solution of Rhodol-OBn(*p*NO_2) or SNARF-OBn(*p*NO_2) were mixed with 1.0 mL of *E. coli* solution (final concentration 10 μM with or without NADPH (1 mM)) and incubated at 37 °C. The fluorescence intensities and fluorescence images of the samples in a 96-well microplate[Greiner Microplate, 655 906, 96-well, PS, F-bottom (chimney well) mCLEAR, black, nonbinding] were monitored at the appropriate reaction time. Rhodol-OBn(*p*NO_2) or SNARF-OBn(*p*NO_2) were excited at 480 or 530 nm and detected at 540 or 600 nm, respectively.

Supporting Information

Supporting Information is available from the Wiley Online Library or from the author.

Acknowledgements

The authors thank Prof. Atsushi Wakamiya (ICR, Kyoto University) and Prof. Tomoya Nakamura (ICR, Kyoto University) for the help with fluorescence quantum yield measurements. This work was supported in part by a Grant-in-Aid for Scientific Research from the Ministry of Education, Culture, Sports, Science and Technology, Japan to E. N. (No. 21710232, 24107513, 26107710, and 24H01129). Y.Y., H.K., and Y.N. contributed equally to this work.

Conflict of Interest

The authors declare no conflict of interest.

Data Availability Statement

The data that support the findings of this study are available in the supplementary material of this article.

Keywords

endogenous nitroreductase, fluorescent probe, lactone formation, self-assembled cluster, turn-on

Received: September 25, 2024
Revised: December 7, 2024
Published online:

[1] a) L. D. Lavis, *Annu. Rev. Biochem.* **2017**, *86*, 825; b) A. P. Demchenko, *Anal. Biochem.* **2005**, *343*, 1.
[2] a) L. D. Lavis, R. T. Raines, *ACS Chem. Biol.* **2014**, *9*, 855; b) J. Chan, S. C. Dodani, C. J. Chang, *Nat. Chem.* **2012**, *4*, 973.
[3] L. D. Lavis, R. T. Raines, *ACS Chem. Biol.* **2008**, *3*, 142.
[4] L. Wang, M. Frei, A. Salim, K. Johnsson, *J. Am. Chem. Soc.* **2019**, *141*, 2770.
[5] S. Keller, M. Kamiya, Y. Urano, *Molecules* **2020**, *25*, 5964.
[6] H. Kobayashi, M. Ogawa, R. Alford, P. L. Choyke, Y. Urano, *Chem. Rev.* **2010**, *110*, 2620.
[7] a) N. Johnsson, K. Johnsson, *ACS Chem. Biol.* **2007**, *2*, 31; b) A. T. Aron, K. M. Ramos-Torres, J. A. Cotruvo, C. J. Chang, *Acc. Chem. Res.* **2015**, *48*, 2434; c) A. Razgulin, N. Ma, J. H. Rao, *Chem. Soc. Rev.* **2011**, *40*, 4186; d) H. Liu, L. Chen, C. Xu, Z. Li, H. Zhang, X. Zhang, W. Tan, *Chem. Soc. Rev.* **2018**, *47*, 7140.
[8] H. Kobayashi, P. Choyke, *Acc. Chem. Res.* **2011**, *44*, 83.
[9] a) K. Kikuchi, H. Takakusa, T. Nagano, *TrAC-Trends Anal. Chem.* **2004**, *23*, 407; b) L. Yuan, W. Lin, K. Zheng, S. Zhu, *Acc. Chem. Res.* **2013**, *46*, 1462; c) X. Huang, J. Song, B. Yung, X. Huang, Y. Xiong, X. Chen, *Chem. Soc. Rev.* **2018**, *47*, 2873; d) Q. Fu, X. Yang, M. Wang, K. Zhu, Y. Wang, J. Song, *ACS Nano* **2024**, *18*, 3916.

[10] a) Y. Urano, D. Asanuma, Y. Hama, Y. Koyama, T. Barrett, M. Kamiya, T. Nagano, T. Watanabe, A. Hasegawa, P. L. Choyke, H. Kobayashi, *Nat. Med.* **2009**, *15*, 104; b) Y. Urano, *Anal. Sci.* **2008**, *24*, 51; c) M. Kamiya, H. Kobayashi, Y. Hama, Y. Koyama, M. Bernardo, T. Nagano, P. L. Choyke, Y. Urano, *J. Am. Chem. Soc.* **2007**, *129*, 3918; d) X. Li, X. Gao, W. Shi, H. Ma, *Chem. Rev.* **2014**, *114*, 590; e) J. Ohata, K. Bruemmer, C. Chang, *Acc. Chem. Res.* **2019**, *52*, 2841; f) S. Gardner, C. Reinhardt, J. Chan, *Angew. Chem., Int. Ed.* **2021**, *60*, 5000; g) A. Yadav, C. Reinhardt, A. Arango, H. Huff, L. Dong, M. Malkowski, A. Das, E. Tajkhorshid, J. Chan, *Angew. Chem., Int. Ed.* **2020**, *59*, 3307.

[11] G. Lukinavicius, L. Reymond, E. D'Este, A. Masharina, F. Gutfert, H. Ta, A. Guether, M. Fournier, S. Rizzo, H. Waldmann, C. Blaukopf, C. Sommer, D. W. Gerlich, H.-D. Arndt, S. W. Hell, K. Johnsson, *Nat. Methods* **2014**, *11*, 731.

[12] a) N. Lardon, L. Wang, A. Tschanz, P. Hoess, M. Tran, E. D'Este, J. Ries, K. Johnsson, *J. Am. Chem. Soc.* **2021**, *143*, 14592; b) G. Lukinavicius, K. Umezawa, N. Olivier, A. Honigmann, G. Yang, T. Plass, V. Mueller, L. Reymond, I. R. Correa, Z.-G. Luo, C. Schultz, E. A. Lemke, P. Heppenstall, C. Eggeling, S. Manley, K. Johnsson, *Nat. Chem.* **2013**, *5*, 132; c) Q. Zheng, A. Ayala, I. Chung, A. Weigel, A. Ranjan, N. Falco, J. Grimm, A. Tkachuk, C. Wu, J. Lippincott-Schwartz, R. Singer, L. Lavis, *ACS Cent. Sci.* **2019**, *5*, 1602; d) Y. Kushida, T. Nagano, K. Hanaoka, *Analyst* **2015**, *140*, 685.

[13] a) K. Mizusawa, Y. Ishida, Y. Takaoka, M. Miyagawa, S. Tsukiji, I. Hamachi, *J. Am. Chem. Soc.* **2010**, *132*, 7291; b) K. Mizusawa, Y. Takaoka, I. Hamachi, *J. Am. Chem. Soc.* **2012**, *134*, 13386; c) T. Yoshii, K. Mizusawa, Y. Takaoka, I. Hamachi, *J. Am. Chem. Soc.* **2014**, *136*, 16635; d) X. Hu, X. Dong, Y. Lu, J. Qi, W. Zhao, W. Wu, *Drug Discovery Today* **2017**, *22*, 382; e) A. Méndez-Ardoy, J. J. Reina, J. Montenegro, *Chem.-Eur. J.* **2020**, *26*, 7516.

[14] J. Qi, X. Hu, X. Dong, Y. Lu, H. Lu, W. Zhao, W. Wu, *Adv. Drug Delivery Rev.* **2019**, *143*, 206.

[15] a) Y. Hong, J. Lam, B. Tang, *Chem. Soc. Rev.* **2011**, *40*, 5361; b) J. Mei, N. Leung, R. Kwok, J. Lam, B. Tang, *Chem. Rev.* **2015**, *115*, 11718; c) S. Suzuki, S. Sasaki, A. Sairi, R. Iwai, B. Tang, G. Konishi, *Angew. Chem., Int. Ed.* **2020**, *59*, 9856; d) F. Würthner, *Angew. Chem., Int. Ed.* **2020**, *59*, 14192.

[16] K. Kokado, K. Sada, *Angew. Chem., Int. Ed.* **2019**, *58*, 8632.

[17] E. Nakata, Y. Yukimachi, Y. Nazumi, M. Uwate, H. Maseda, Y. Uto, T. Hashimoto, Y. Okamoto, H. Hori, T. Morii, *RSC Adv.* **2014**, *4*, 348.

[18] E. Nakata, K. Gerelbaatar, F. Komatsubara, T. Morii, *Molecules* **2022**, *27*, 7181.

[19] E. Nakata, Y. Yukimachi, Y. Uto, H. Hori, T. Morii, *Sci. Technol. Adv. Mater.* **2016**, *17*, 431.

[20] a) E. Nakata, Y. Nazumi, Y. Yukimachi, Y. Uto, H. Maezawa, T. Hashimoto, Y. Okamoto, H. Hori, *Bioorg. Med. Chem. Lett.* **2011**, *21*, 1663; b) E. Nakata, Y. Yukimachi, Y. Nazumi, Y. Uto, T. Hashimoto, Y. Okamoto, H. Hori, *Chem. Lett.* **2010**, *39*, 734; c) T. Liu, X. Li, Y. Qiu, Y. Zhao, X. Luo, G. Liu, Q. Sun, *Dyes Pigm.* **2024**, *222*, 111872; d) C. Richter, C. Schneider, M. Quick, P. Volz, R. Mahrwald, J. Hughes, B. Dick, U. Alexiev, N. Ernsting, *Phys. Chem. Chem. Phys.* **2015**, *17*, 30590; e) Y. Poronik, K. Vygranenko, D. Gryko, D. Gryko, *Chem. Soc. Rev.* **2019**, *48*, 5242.

[21] J. Whitaker, R. Haugland, F. Prendergast, *Anal. Biochem.* **1991**, *194*, 330.

[22] J. Y. Han, K. Burgess, *Chem. Rev.* **2010**, *110*, 2709.

[23] E. Nakata, Y. Yukimachi, Y. Nazumi, Y. Uto, H. Maezawa, T. Hashimoto, Y. Okamoto, H. Hori, *Chem. Commun.* **2010**, *46*, 3526.

[24] E. Nakata, Y. Nazumi, Y. Yukimachi, Y. Uto, H. Hori, T. Morii, *Bull. Chem. Soc. Jpn.* **2015**, *88*, 327.

[25] E. Nakata, Y. Yukimachi, H. Kariyazono, S. Im, C. Abe, Y. Uto, H. Maezawa, T. Hashimoto, Y. Okamoto, H. Hori, *Bioorg. Med. Chem.* **2009**, *17*, 6952.

[26] O. Valdesaguilera, D. Neckers, *Acc. Chem. Res.* **1989**, *22*, 171.

[27] a) R. Boddu, O. Perumal, K. Divakar, *Biotechnol. Appl. Biochem.* **2021**, *68*, 1518; b) M. Chen, D. Chen, P. Chou, *ChemPlusChem* **2021**, *86*, 11; c) W. Chyan, R. Raines, *ACS Chem. Biol.* **2018**, *13*, 1810; d) S. Das, H. Indurthi, P. Asati, D. Sharma, *ChemistrySelect* **2022**, *7*, 202102895; e) A. Schena, K. Johnsson, *Angew. Chem., Int. Ed.* **2014**, *53*, 1302; f) Y. Qi, L. Guo, L. Chen, H. Li, Y. Yang, A. Jiang, H. Zhu, *Coord. Chem. Rev.* **2020**, *421*, 213460; g) X. Wu, W. Shi, X. Li, H. Ma, *Acc. Chem. Res.* **2019**, *52*, 1892; h) L. Yao, C. Yin, F. Huo, *Micromachines* **2022**, *13*, 1328; i) K. Singh, A. Rotaru, A. Beharry, *ACS Chem. Biol.* **2018**, *13*, 1785; j) S. Yoon, S. Park, Y. Cha, L. Gopala, M. Lee, *Front. Chem.* **2021**, *9*, 743923; k) Y. Yang, H. Zhai, J. Yuan, K. Wang, H. Zhang, *Chem.-Asian J* **2022**, *17*, 202200043; l) J. Qiao, M. Wang, M. Cui, Y. Fang, H. Li, C. Zheng, Z. Li, Y. Xu, H. Hua, D. Li, *J. Pharm. Biomed. Anal.* **2021**, *203*, 114199.

[28] Z. Cao, W. Li, R. Liu, X. Li, H. Li, L. Liu, Y. Chen, C. Lv, Y. Liu, *Biomed. Pharmacother.* **2019**, *118*, 109340.

[29] G. Prosser, J. Copp, S. Syddall, E. Williams, J. Smaill, W. Wilson, A. Patterson, D. Ackerley, *Biochem. Pharmacol.* **2010**, *79*, 678.

[30] J. Copp, E. Williams, M. Rich, A. Patterson, J. Smaill, D. Ackerley, *Protein Eng., Des. Sel.* **2014**, *27*, 399.

[31] M. Roldan, E. Perez-Reinado, F. Castillo, C. Moreno-Vivian, *FEMS Microbiol. Rev.* **2008**, *32*, 474.

[32] a) G. Prosser, J. Copp, A. Mowday, C. Guise, S. Syddall, E. Williams, C. Horvat, P. Swe, A. Ashoorzadeh, W. Denny, J. Smaill, A. Patterson, D. Ackerley, *Biochem. Pharmacol.* **2013**, *85*, 1091; b) E. Williams, R. Little, A. Mowday, M. Rich, J. Chan-Hyams, J. Copp, J. Smaill, A. Patterson, D. Ackerley, *Biochem. J.* **2015**, *471*, 131; c) M. Day, D. Jarrom, N. Rajah, P. Searle, E. Hyde, S. White, *Proteins: Struct., Funct., Bioinf* **2023**, *91*, 585.

[33] S. Zenno, H. Koike, M. Tanokura, K. Saigo, *J. Biochem.* **1996**, *120*, 736.

[34] a) S. Zenno, H. Koike, A. Kumar, R. Jayaraman, M. Tanokura, K. Saigo, *J. Bacteriol.* **1996**, *178*, 4508; b) A. Sharrock, S. McManaway, M. Rich, J. Mumm, I. Hermans, M. Tercel, F. Pruijn, D. Ackerley, *Front. Pharmacol.* **2021**, *12*, 701456.

[35] A. Valle, S. Le Borgne, J. Bolívar, G. Cabrera, D. Cantero, *Appl. Microbiol. Biotechnol.* **2012**, *94*, 163.

[36] W. R. Miller, C. A. Arias, *Nat. Rev. Microbiol.* **2024**, *22*, 598.

[37] Y.-L. Qi, L. Guo, L.-L. Chen, H. Li, Y.-S. Yang, A.-Q. Jiang, H.-L. Zhu, *Coord. Chem. Rev.* **2020**, *421*, 213460.

[38] R. S. Boddu, O. Perumal, K. Divakar, *Biotechnol. Appl. Biochem.* **2021**, *68*, 1518.

[39] S. Verma, N. Sigla, S. S. Bhadwai, R. Chouhan, S. Kumar, S. G. Gandhi, S. Kaur, *ChemistrySelect* **2024**, *9*, 202401426.

[40] J. A. Myers, B. S. Curtis, W. R. Curtis, *BMC Biophys* **2013**, *6*, 4.